

# Microstructure evolution and precipitation behavior of Al-Mg-Si alloy during initial aging

\*Ya-ya Zheng<sup>1,3</sup>, Bing-hui Luo<sup>2</sup>, Wei Xie<sup>3</sup>, and Wang Li<sup>1</sup>

1. Department of Materials Engineering, Hunan University of Humanities, Science and Technology, Loudi 417000, Hunan, China

2. College of Materials Science and Engineering, Central South University, Changsha 410083, China

3. Key Laboratory of Safety Design and Reliability Technology for Engineering Vehicle, Changsha University of Science & Technology, Changsha 410114, China

**Abstract:** The microstructure evolution and precipitation behavior of Al-Mg-Si alloy during initial aging were studied using hardness testing, conductivity testing, differential scanning calorimetry (DSC), and high resolution transmission electron microscopy (HRTEM). The results show that the precipitation sequence of the Al-Mg-Si alloy during initial aging can be represented as: supersaturated solid solution → spherical Mg/Si clusters → needle-like Guinier Preston (GP) zone →  $\beta''$ . Clusters are completely coherent with the Al matrix. The GP zone with relatively complete independent lattice parameters that differ slightly from the Al matrix parameters, is oriented along the direction of  $\langle 111 \rangle_{\text{Al}}$  and lying on  $\{111\}_{\text{Al}}$  plane. The strength of the Al-Mg-Si alloy is greatly enhanced by the three-dimensional strain field that exists between the  $\beta''$  phase and the two  $\{200\}_{\text{Al}}$  planes. After aging at 170 °C for 6 h, the hardness reaches the peak of 127 HV and remains for a long time. At this stage, the electrical conductivity keeps relatively stable due to the formation of coherent precipitates (Mg/Si clusters/GP zones) and the reduction in solute atom concentration in the Al matrix. The severe coarsening and decreased number density of the  $\beta''$  phase during the over-aging stage result in a significant decrease in the hardness.

**Keywords:** Al-Mg-Si alloy; precipitation behavior; strengthening mechanism; strain field;  $\beta''$

CLC numbers: TG146.21

Document code: A

Article ID: 1672-6421(2023)01-057-06

## 1 Introduction

Al-Mg-Si alloys, as heat-treatable and high-performance aluminum alloys, have been extensively employed as lightweight materials in aerospace, rail transport, and automotive applications<sup>[1,2]</sup>. Their mechanical properties are primarily achieved through the precipitation of metastable strengthening phases during artificial aging<sup>[3,4]</sup>. The generally accepted precipitation sequence of the Al-Mg-Si alloy can be expressed as<sup>[5-7]</sup>: super saturated solid solution (SSSS) → Guinier Preston zone (GP zone) →  $\beta''$  →  $\beta'$  →  $\beta(\text{Mg}_2\text{Si})$ . GP zones formed during the early aging stage by clustering solution atoms and retained coherent interactions with the matrix, resulting in significant strain fields near the coherent interface<sup>[8]</sup>. This severe lattice distortion inhibits dislocation movement and increases the alloy's hardness. The needle-shaped  $\beta''$  phase is considered as the most important strengthening

phase<sup>[9]</sup>. As the aging process progresses,  $\beta''$  evolves into  $\beta'$  phase with a semi-coherent interaction with the Al matrix, resulting in a reduction in mechanical properties<sup>[10,11]</sup>. The type, distribution, density, and structural characteristics of the precipitates are critical to the overall properties of the alloy.

Thus, extensive research has been conducted to optimize mechanical properties, with a particular emphasis on nanometer-scale metastable phases that precipitate during the initial aging or at the peak-aging state<sup>[12-16]</sup>. Kim et al.<sup>[17]</sup> through theoretical analysis and calculations, found that most clusters in the early aging stage exist in the form of spheres. Du et al.<sup>[18]</sup> discovered that some clusters associated with needle-like. Ding et al.<sup>[19]</sup> used HRTEM to observe the existence of the GP zone, and considered that the GP zone provided a nucleation site for  $\beta''$ . Wen et al.<sup>[20]</sup> concluded that the  $\beta''$  phase had a monoclinic structure. Edwards et al.<sup>[21]</sup> studied the structure of precipitates during early aging, suggesting that  $\beta''$  had a base-centered monoclinic structure. Allen et al.<sup>[22]</sup> reported the precipitation of needle-like phase with an unknown crystal structure during initial aging. Yang et al.<sup>[23]</sup> concluded that  $\beta''$  precipitate lattice parameters were  $a=6.50 \text{ \AA}$ ,  $c=7.60 \text{ \AA}$ ,

### \*Ya-ya Zheng

Male, born in 1990, Ph. D. His research interests mainly focus on the microstructures and comprehensive properties of Al alloys.

E-mail: yayazhengcsu@163.com

Received: 2021-11-01; Accepted: 2022-10-02

$\gamma=70^\circ$ . Jin et al. [24] studied the structure of small precipitates by 3DAP, and suggested that  $\beta''$  phase lattice parameters were  $a=15.1 \text{ \AA}$ ,  $c=0.67 \text{ \AA}$ ,  $\beta=105^\circ$ . It can be seen that, despite the fact that various studies have reported information regarding the precipitation phase during the early stages of aging, the results remain equivocal or contradictory. The precipitation sequence, as well as the evolution of the initial precipitates' shape and structural features, has yet to be determined.

To fully understand the evolution of initial precipitates as well as their structural characteristics, it is necessary inevitable to obtain a detailed understanding of the precipitation behavior of the Al-Mg-Si alloy during initial aging. It should be pointed out that the  $\beta'$  phase and subsequent phases are rather accessible to characterize as they already have specific chemical components and structures [6,7]. Consequently, the purpose of this study is to clarify the microstructure evolution and precipitation behavior of an Al-Mg-Si alloy during initial aging.

## 2 Material and methods

The alloy used in the experiment was designed and then manufactured using the traditional casting procedure. In an electric resistance furnace, pure metal Al, Al-20wt.%Si, Al-20wt.%Mn, Al-5wt.%Ti, and Al-3.9wt.%Cr master alloys were melted at  $750^\circ\text{C}$ . After holding for 1.5 h, pure Mg and Ag were added to the melt under an argon environment. To achieve adequate homogenized diffusion of alloying components, the melt was agitated discontinuously at  $750^\circ\text{C}$  for 60 min. Finally, before pouring the melt into an iron mold, the temperature was maintained at  $725^\circ\text{C}$  for 30 min. The as-cast ingot was homogenized at  $520^\circ\text{C}$  for 24 h before being air-cooled to room temperature. Table 1 displays the chemical composition of the alloy determined by an optical emission spectrometer. To create supersaturated solid solutions, samples ( $30\times 30\times 30 \text{ mm}^3$  in size) were cut from the homogenized ingots and then solution heat treated at  $520^\circ\text{C}$  for 2 h, followed by water quenching. Then, the samples were subjected to aging treatment at  $170^\circ\text{C}$  for different times from 10 min to 1,300 min. In order to prevent the negative effects caused by natural aging, the sample was placed in liquid nitrogen immediately after quenching.

The hardness testing was conducted on the HV-1000 Vickers hardness tester. The load was 200 g, and the dwelling

Table 1: Chemical compositions of Al-Mg-Si alloy (wt.%)

Mg	Si	Mn	Cr	Ti	Ag	Al
1.2	1.1	0.15	0.15	0.15	0.1	Bal.

time was 15 s. Each sample was measured 5 times at different positions, and the average hardness of the testing was taken as the final hardness. The DSC test was performed using a Mettler-1100LF synchronous thermal analyzer. The test sample was a flake with a thickness of 2 mm. The temperature range was from  $20^\circ\text{C}$  to  $680^\circ\text{C}$ , with an  $8^\circ\text{C}\cdot\text{min}^{-1}$  heating rate, and argon as a protective gas. The phase transformation process was analyzed by DSC data. The TEM and HRTEM characterization was performed on a FEI Tecnai G<sup>2</sup> F20 transmission electron microscope. TEM specimens were prepared using a typical twin jet electro polishing equipment with a standard solution of 30% HNO<sub>3</sub> in methanol at  $-28^\circ\text{C}$ . To prevent the microstructure from being corroded by the residual corrosive liquid, the sample was immediately immersed in alcohol and cleaned several times.

## 3 Results and discussion

### 3.1 Age-hardening and electrical conductivity variation

Figure 1 presents the hardness and electrical conductivity variation curves of an Al-Mg-Si alloy aged at  $170^\circ\text{C}$  for various aging times. Region A represents the under-aging stage of the alloy, during which the alloy's hardness and electrical conductivity improve significantly as aging time increases. Region B represents the plateau period of peak hardness, and the peak hardness of 127 HV is achieved after aging for  $170^\circ\text{C}/6 \text{ h}$ . At this stage, the electrical conductivity is in a relatively stable state, with a slight downward trend. Region C represents the over-aging stage where the hardness begins to decrease and the electrical conductivity presents an upward trend.

### 3.2 DSC analysis

Figure 2 shows DSC flow curves of Al-Mg-Si alloys in different states after heat treatment. As a reference, a solution quenched

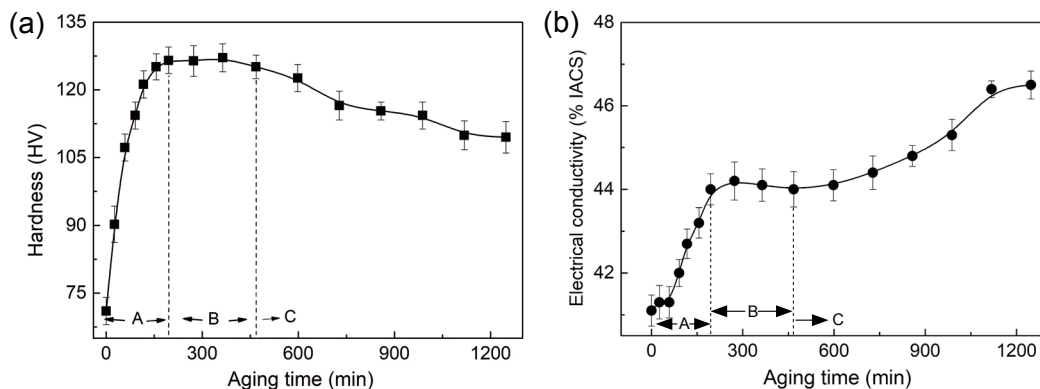


Fig. 1: Variation of hardness (a) and electrical conductivity (b) of Al-Mg-Si alloys during aging at  $170^\circ\text{C}$  for different times

sample was also tested. The three curves all show obvious characteristics: exothermic peaks and endothermic peaks. However, the peak intensity and peak position have undergone significant changes and shifts. For the solid solution samples, the precipitation peak at around 100 °C is related to the formation of cluster and GP zone, and the endothermic peak at around 225 °C is produced by the precipitation of  $\beta''$  phase. The DSC curve of under-aging sample is similar to that of the solution quenched sample, but the formation peak of the cluster/GP zone is weaker, owing to lesser saturation of solute atoms in the under-aging alloy. For the peak-aging sample, the precipitation of strengthening phases significantly reduces the concentration of solute atoms, resulting in the disappearance of the formation peak of clusters and GP zones. Furthermore, when compared to an under-aging sample, the endothermic and exothermic peaks corresponding to  $\beta''$  of the peaking sample have shifted to a higher temperature, indicating that the stability of  $\beta''$  phase of the peak-aging sample rises and the dissolution process delays.

### 3.3 Microstructure evolution

Figure 3 shows TEM images and the corresponding selected area electron diffraction pattern (SADP) of the investigated alloys after aging at 170 °C for different times. With the exception of the diffraction spots of the Al matrix and the strong strain field in the accompanying SADP, no other diffraction contrast is detected in Fig. 3(a). In addition, the

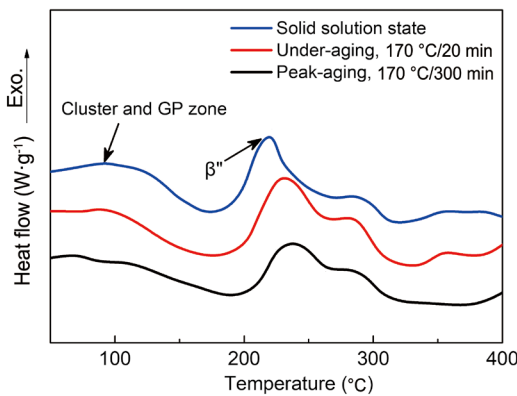


Fig. 2: DSC analysis of specimens after heat-treatment at various conditions

hardness curve shows a significant increase after aging at 170 °C for 20 min, suggesting the precipitation of clusters. Elements such as Mg and Si occupy the lattice sites of Al atoms to form these clusters, resulting in strain fields surrounding the clusters [25]. However, no obvious diffraction spots indicating the generation of these clusters can be seen in the conventional TEM image due to the small size of the cluster. As the aging time increases to 60 min, a large number of needle-like phases appear in the grain. Based on the morphology of the precipitates and the representative "cross-shaped" diffractions in SADP, the needle-like phase can be identified as  $\beta''$  phase.

When the alloy is further aged to 300 min, two types of precipitates with different morphologies and sizes are formed. One is small-sized precipitates, possibly clusters or GP zones. The other is the needle-like  $\beta''$  phase with a size of about 19 nm, lying in the directions of  $\langle 100 \rangle_{Al}$  and  $\langle 010 \rangle_{Al}$ . Additionally, there is a massively embedded  $\beta''$  phase with the long axis direction parallel to the viewing direction. The corresponding SADP exhibits characteristic "cross-shaped" diffractions and Al matrix spots, suggesting that the volume percentage of  $\beta''$  phase reaches a certain level. The generation of these "cross-shaped" diffractions originates from high-order diffraction spots. Because their diffraction originates from the high-order index belt axis, the diffraction strength is relatively weaker.

In addition, by combining the evolution of the alloy's precipitation behavior, how the alloy's electrical conductivity changes with aging time can be concluded. It is generally accepted that the electrical conductivity of metal materials is influenced by the interaction of transferring electrons with scattering centers provided by strain fields in the crystalline matrix [26, 27]. An increase in electrical conductivity would arise from a decrease in scattering centers. For Al alloys, the scattering center is mostly generated by the strain field around the precipitate. At the beginning of aging, the formation of precipitates gradually reduces the concentration of solute atoms in the aluminum matrix, greatly increasing the electrical conductivity. When the aging time is extended to 300 min, the change in conductivity is caused by a combination of two factors. One factor is that the formation of coherent

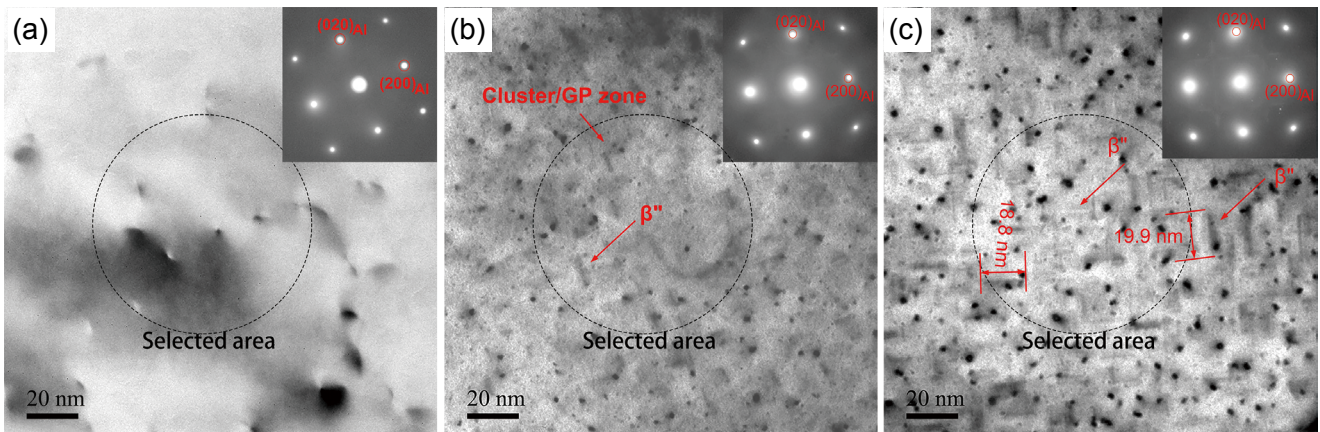


Fig. 3: TEM image of Al-Mg-Si alloys aging at 170 °C for different times along the  $[001]_{Al}$  axis: (a) 20 min; (b) 60 min; (c) 300 min

precipitates (Mg/Si clusters/GP zones) enhances resistivity. The other factor is the increase in electrical conductivity caused by the formation of Mg/Si clusters/GP zones and the decrease in solute atom concentration. As aging progresses, the coarsening of the main strengthening phase decreases the strain field surrounding the precipitates, resulting in a continuous rise in electrical conductivity.

In order to further determine the precipitation behavior of the alloy during aging, Fig. 4 shows the HRTEM images of typical precipitates of Al-Mg-Si alloys aged at 170 °C for different times and corresponding fast Fourier transform (FFT). In the initial stage of aging, a large number of spherical clusters with a size of less than 3 nm are precipitated [Figs. 4(a, d)]. As the aging time increases, the clusters grow continuously by absorbing the surrounding solute atoms such as Mg and Si

[Figs. 4(b, e)] and evolve into needle-like phases. According to the coherent state with the matrix and its size and morphology characteristics, it can be inferred that the precipitates are GP zones<sup>[9]</sup>. The GP zone is located on the  $\{111\}_{Al}$  plane and extends in the direction of  $\langle 111 \rangle_{Al}$ . The corresponding FFT shows significant diffraction fringes on the Al matrix point that are slightly deviated from the  $\langle 100 \rangle_{Al}$  direction, demonstrating that the GP zone already has relatively complete independent lattice parameters. As the aging progresses, the GP zone phase acts as the nucleation site for the  $\beta''$  phase, and in the peak-aging state [Figs. 4(c, f)], further grows towards the  $\beta''$  phase with monoclinic structure. As a result, the precipitation sequence of Al-Mg-Si alloy during initial aging can be expressed as: spherical atomic cluster evolves into needle-like GP zone, and needle-like GP zone evolves into  $\beta''$ .

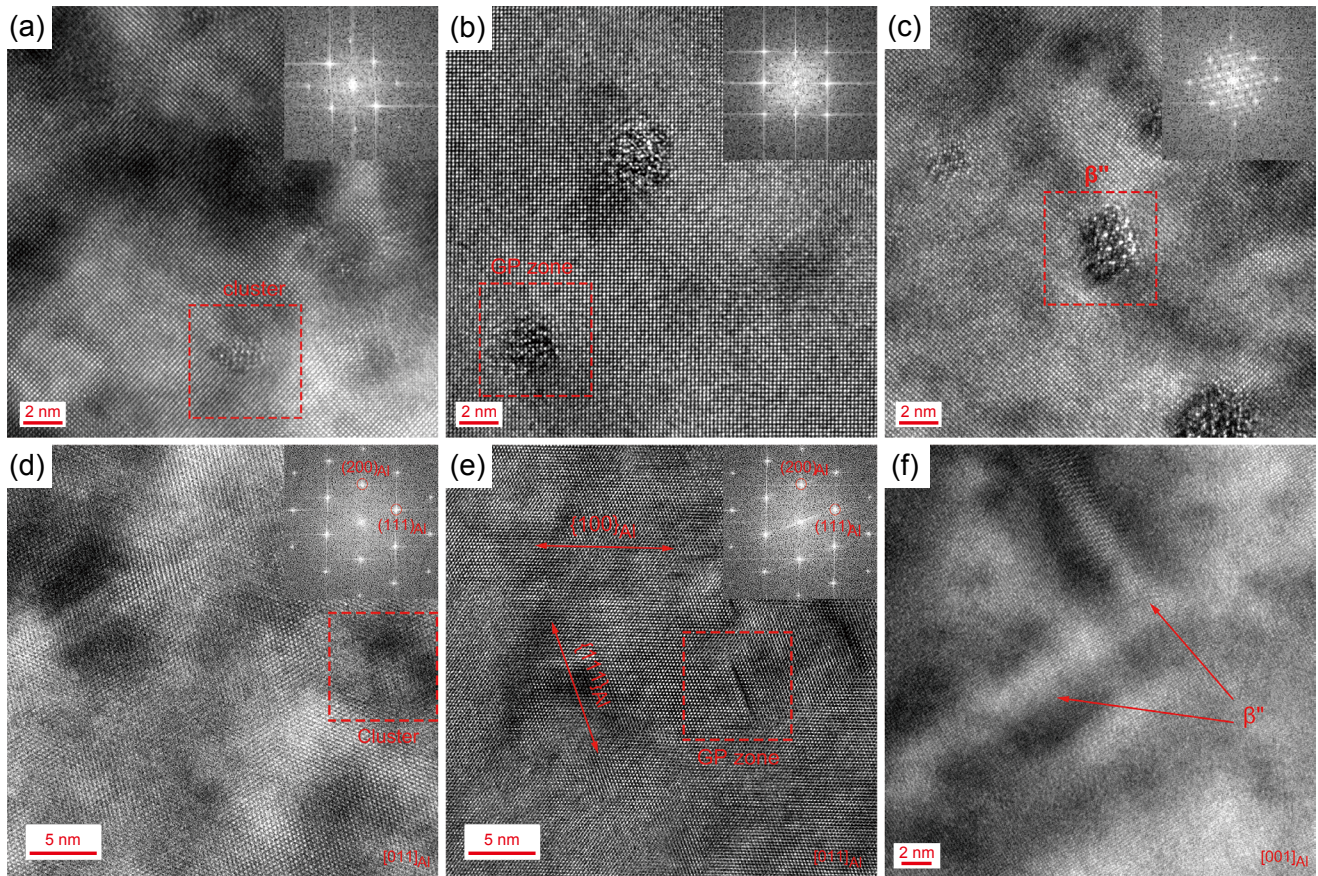


Fig. 4: HRTEM images of typical precipitate in Al-Mg-Si alloy with different aging conditions and corresponding FFT patterns: (a, d) under-aging, 170 °C/10 min; (b, e) under-aging, 170 °C/20 min; (c, f) peak-aging, 170 °C/300 min

Figure 5 shows the HRTEM images of the needle-like  $\beta''$  phase, embedded  $\beta''$  phase and the corresponding FFTs. It can be seen from Figs. 5(a, b) that the  $\beta''$  phase belongs to the polygonal monoclinic crystal system, and the lattice parameters are  $a=1.51$  nm,  $c=0.67$  nm,  $\beta=105.3^\circ$ . The orientation relationship with the Al matrix is:  $(010)_{\beta''}/(001)_{Al}$ ,  $[001]_{\beta''}/[310]_{Al}$  and  $[100]_{\beta''}/[230]_{Al}$ . The  $\beta''$  phase size is about 25 nm. The long axis direction shows a highly coherent relationship with the Al matrix, and an obvious coherent strain contrast appears at the interface [Fig. 5(c)]. A large number of Mg and Si atoms are enriched in the  $\beta''$  phase [Fig. 5(e)].

The atomic radius of magnesium and silicon is 0.160 nm and 0.134 nm, respectively, while that of aluminum is 0.143 nm. There is a significant difference in radius between the atoms, which inevitably leads to the presence of coherent strain at the interface surrounding the precipitates. As shown in Fig. 5(d), a three-dimensional strain field around the interface between the  $\beta''$  and the two  $\{200\}_{Al}$  planes causes the distortion of the aluminum lattice, which can effectively inhibit the movement of dislocations. Therefore, the  $\beta''$  phase has a significant strengthening effect, and the strengthening effect increases with the increase of the coherent strain field between  $\beta''$  and the Al matrix.

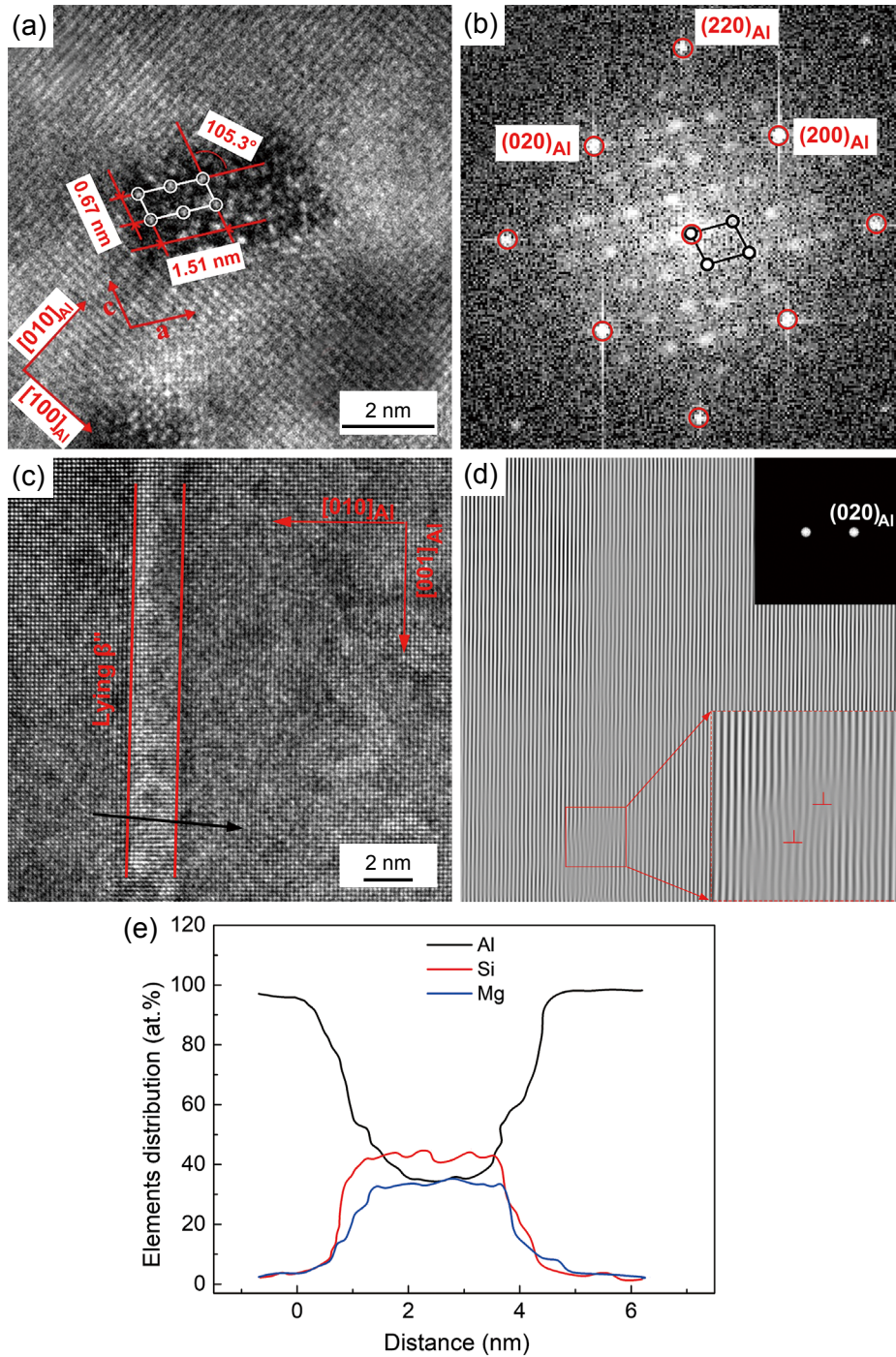


Fig. 5: HRTEM images of the  $\beta''$  phase and corresponding FFT and IFFT pattern: (a) lying  $\beta''$  along  $[001]_{Al}$ ; (b, c, d) embedded  $\beta''$ , and the corresponding FFT and IFFT pattern, respectively; (e) compositional line profile across the embedded  $\beta''$  phase along the black arrow in (c)

## 4 Conclusions

(1) Precipitation sequence of the Al-Mg-Si alloy in initial aging can be expressed as: supersaturated solid solution  $\rightarrow$  spherical Mg/Si cluster  $\rightarrow$  needle-like GP zone  $\rightarrow$   $\beta''$  phase. The cluster is completely coherent with the matrix. The GP zone with relatively complete independent lattice parameters that differ slightly from the Al matrix parameters, is oriented along the direction of  $\langle 111 \rangle_{Al}$  and lies on  $\{111\}_{Al}$  plane.

(2) After aging at 170 °C for 6 h, the alloy reaches a peak hardness of 127 HV which remains for a long time. At this

stage, the electrical conductivity stays relatively stable due to the combination of effects such as the formation of coherent precipitates (Mg/Si clusters/GP zones) and a reduction in solute atom concentration in the Al matrix.

(3) The existence of three-dimensional coherent strain at the interface between the  $\beta''$  phase and the two  $\{200\}_{Al}$  planes provides an important contribution to the strengthening of the Al-Mg-Si alloy. In the over-aging state, the  $\beta''$  phase becomes coarser, and the hardness of the alloy decreases significantly.

## Acknowledgement

The work was financially supported by the Research Foundation of Education Bureau Hunan Province, China (Grant No. 22C0598).

## Conflict of interest

The authors declare that they have no conflict of interest.

## References

- [1] Wang D T, Zhang X Z, Xu S S, et al. Improvement of mechanical properties in micro-alloying Al-Si-Mg-Zn cast alloy. *Materials Letters*, 2021, 283(15): 128810.
- [2] Meng F B, Huang H J, Yuan X G, et al. Segregation in squeeze casting 6061 aluminum alloy wheel spokes and its formation mechanism. *China Foundry*, 2021, 18(1): 45–51.
- [3] Chen B, Zhang C H, Jin Y. First-principles calculation of interface binding strength and fracture performance of  $\beta'$ /Al interface in Al-Mg-Si-Cu alloy. *Journal of Alloys & Compounds*, 2020, 830: 154515.
- [4] Lai Y X, Fan W, Yin M J, et al. Structures and formation mechanisms of dislocation-induced precipitates in relation to the age-hardening responses of Al-Mg-Si alloys. *Journal of Materials Science & Technology*, 2020, 41: 127–138.
- [5] Zhu S Q, Shi H C, Cui X Y, et al. Design of solute clustering during thermomechanical processing of AA6016 Al-Mg-Si alloy. *Acta Materialia*, 2021, 203: 1359–6454.
- [6] Gupta A K, Lloyd D J, Court S A. Precipitation hardening processes in an Al-0.4%Mg-1.3%Si-0.25%Fe aluminum alloy. *Materials Science & Engineering A*, 2001, 301(2): 140–146.
- [7] Zhen L, Kang S B. DSC analyses of the precipitation behavior of two Al-Mg-Si alloys naturally aged for different times. *Materials Letters*, 1998, 37(6): 349–353.
- [8] Aluru P S, Ashim B M, Debdulal D. Mechanical properties and corrosion behavior of artificially aged Al-Mg-Si alloy. *Journal of Materials Research and Technology*, 2020, 9(1): 1005–1024.
- [9] Aruga Y, Kozuka M, Takaki Y, et al. Formation and reversion of clusters during natural aging and subsequent artificial aging in an Al-Mg-Si alloy. *Materials Science & Engineering A*, 2015, 631(17): 86–96.
- [10] Liu M, Banhart J. Effect of Cu and Ge on solute clustering in Al-Mg-Si alloys. *Materials Science & Engineering A*, 2016, 658(21): 238–245.
- [11] Kumar N, Jayaganthan R, Brokmeier H G. Effect of deformation temperature on precipitation, microstructural evolution, mechanical and corrosion behavior of 6082 Al alloy. *Transactions of Nonferrous Metals Society of China*, 2017, 27(3): 475–492.
- [12] Murayama M, Hono K, Saga M, et al. Atom probe studies on the early stages of precipitation in Al-Mg-Si alloys. *Materials Science & Engineering A*, 1998, 250(1): 127–132.
- [13] Mørtzell E V A, Marioara C D, Andersen S J, et al. Effects of germanium, copper, and silver substitutions on hardness and microstructure in lean Al-Mg-Si alloys. *Metallurgical & Materials Transactions A*, 2015, 46(6): 4369–4379.
- [14] Deng L, Zhang X M, Tang J F, et al. First-principles study of the binding preferences and diffusion behaviors of solutes in vanadium alloys. *Journal of Alloys & Compounds*, 2016, 660(5): 55–61.
- [15] Messina L, Malerba L, Olsson P. Stability and mobility of small vacancy-solute complexes in Fe-MnNi and dilute Fe-X alloys: A kinetic Monte Carlo study. *Nuclear Instruments and Methods in Physics Research, Section B: Beam Interactions with Materials and Atoms*, 2015, 352(1): 61–66.
- [16] Li H, Wang J Y, Jiang H T, et al. Characterizations of precipitation behavior of Al-Mg-Si alloys under different heat treatments. *China Foundry*, 2018, 15(2): 89–96.
- [17] Kim J, Hayashi M, Kobayashi E, et al. Influence of Si addition on quenching sensitivity and formation of nano-precipitate in Al-Mg-Si alloys. *Journal of Nanoscience & Nanotechnology*, 2016, 16(2): 1814–1817.
- [18] Du J L, Zhang A, Zhang Y B, et al. Atomistic determination on stability, cluster and microstructures in terms of crystallographic and thermo-kinetic integration of Al-Mg-Si alloys. *Materials Today Communications*, 2020, 24: 101220.
- [19] Ding L P, Jia Z H, Nie J F, et al. The structural and compositional evolution of precipitates in Al-Mg-Si-Cu alloy. *Acta Materialia*, 2018, 145: 437–450.
- [20] Weng Y Y, Ding L P, Zhang Z H, et al. Effect of Ag addition on the precipitation evolution and interfacial segregation for Al-Mg-Si alloy. *Acta Materialia*, 2019, 180: 301–316.
- [21] Edwards G A, Stiller K, Dunlop G L, et al. The precipitation sequence in Al-Mg-Si alloys. *Acta Materialia*, 1998, 46(11): 3893–3904.
- [22] Dutta I, Allen S M, Hafley J L. Effect of reinforcement on the aging response of cast 6061 Al-Al<sub>2</sub>O<sub>3</sub> particulate composites. *Metallurgical & Materials Transactions A*, 1991, 22: 2553–2563.
- [23] Yang W, Wang M, Jia Y, et al. Studies of orientations of  $\beta''$  precipitates in Al-Mg-Si-(Cu) alloys by electron diffraction and transition matrix analysis. *Metallurgical & Materials Transactions A*, 2011, 42: 2917–2929.
- [24] Jin M, Li J, Shao G J. The effects of Cu addition on the microstructure and thermal stability of an Al-Mg-Si alloy. *Journal of Alloys & Compounds*, 2007, 437(1–2): 146–150.
- [25] Yang Z, Jiang X H, Zhang X P, et al. Natural ageing clustering under different quenching conditions in an Al-Mg-Si alloy. *Scripta Materialia*, 2021, 190: 179–182.
- [26] Hesam P, Mohammad R J, Gholamreza K. Constrained groove pressing and subsequent annealing of Al-Mn-Si alloy: Microstructure evolutions, crystallographic transformations, mechanical properties, electrical conductivity and corrosion resistance. *Corrosion Science*, 2017, 124: 34–46.
- [27] Liu T, Yin Y S, Chen S G, et al. Super-hydrophobic surfaces improve corrosion resistance of copper in seawater. *Electrochimica Acta*, 2007, 52: 3709–3713.